Conformable and robust microfluidic force sensors to enable precision joint replacement surgery

Supporting Information

Liam Ives [a], Alizée Pace [a], Fabian Bor [a], Qingshen Jing [a], Tom Wade [a], Jehangir Cama *[b-d], Vikas Khanduja *[e], and Sohini Kar-Narayan *[a]

[a] Department of Materials Science and Metallurgy, University of Cambridge, 27 Charles Babbage Road, Cambridge CB3 0FS, UK.

[b] Cavendish Laboratory, Department of Physics, University of Cambridge, JJ Thomson Avenue, Cambridge CB3 0HE, UK.

[c] Living Systems Institute, University of Exeter, Stocker Road, Exeter EX4 4QD, UK.

[d] College of Engineering, Mathematics and Physical Sciences, Harrison Building, University of Exeter, North Park Road, Exeter EX4 4QF, UK

[e] Cambridge Young Adult Hip Service, Addenbrooke's, Cambridge University Hospitals, Box 37, Hills Road, Cambridge CB2 0QQ, UK

*Corresponding authors. Email: j.cama@exeter.ac.uk, vk279@cam.ac.uk, sk568@cam.ac.uk

Materials and Methods

Component	Material (simulations)	Material (experimental validation)	Notes
Microfluidic chip	PDMS, Flexible Resin	PDMS, Flexible Resin	
Mold for PDMS microfluidic chip	-	Clear Resin	Flexible Resin microfluidic chips are directly 3D-printed and so do not require a mold
Liquid	Glycerol:DI water (2:1 by volume)	Glycerol:DI water (2:1 by volume)	
Electrode layer	Electrodes: silver	Substrate: polyimide sheet (Kapton) Electrodes: silver	
Femoral head	Alumina	Alumina	
Femoral stem	-	Aluminium	
Insert	HDPE	Durable Resin	UHMWPE used in THR
Bespoke mechanical testing rig	-	Polycarbonate base with brass rotating stage	

Table S1.

List of components and materials used in FEM and mechanical testing.

Experimental Mechanical Characterisation of Sensor and Trial Insert Materials

Examples of candidate materials for the microfluidic chip include polydimethylsiloxane (PDMS) and “Flexible Resin” (Formlabs, USA), a stereolithography (SLA) 3D printing resin. Flexible Resin has a larger hardness (Shore A hardness = 80-85 [1]) than PDMS (approx. Shore A hardness = 44 at room temperature [2]) and is therefore likely to be stiffer. Formlabs do not reveal the exact composition of Flexible Resin, so mechanical characterisation was done to determine its suitability over PDMS.

While PDMS is one of the materials used to construct the channel and reservoir in this paper, it has many limitations for this application. It absorbs small molecules, decreasing the volume of fluid in the reservoir and making the sensor more susceptible to air bubble intrusion [3–5]. There is some variability between the mechanical properties of different batches of PDMS, as it heavily depends on the extent of mixing that occurs, the curing temperature and curing duration. Therefore, some attempt has been made to find suitable alternatives to PDMS. The desired criteria are for a material that (i) can withstand forces up to similar loads applied by surgeons, estimated to be in the range of hundreds of Newtons, (ii) has an appropriate stiffness such that at these forces the reservoir is mostly depleted (for maximum sensitivity) and (iii) has a scalable manufacturing process.

Some candidate materials are available in the library of Engineering Resins available from Formlabs for their SLA printers (Formlabs, USA). SLA printing is already established to have good scalability and high resolution [6]. Some possible resins include the Flexible, Elastic, Durable and Tough resins. The exact chemical compositions are unknown due to their proprietary nature, but some mechanical properties have been provided by Formlabs, who have suggested materials that are similar to these resins (PMMA is similar to Grey Resin, for example).

The mechanical properties of PDMS, Flexible Resin and Durable Resin were characterised. Dog-bone shaped samples were used for tensile testing, with dimensions corresponding to the American Society for Testing and Materials (ASTM) standard D412-C, and were prepared in a laser-cut poly(methyl methacrylate) mold (for PDMS) or direct stereolithography 3D printing using the Formlabs Form 3 3D printer (for Flexible Resin, Durable Resin). Compressive testing samples consisted of 10 mm diameter, 10 mm height cylinders, as in ASTM D575-91 [7], and were molded in a drilled PMMA sheet (for PDMS) or SLA printed (for Flexible Resin and Durable Resin). For the PDMS samples, PDMS (Sylgard 184, Dow, USA) was mixed with curing agent in a 10:1 ratio by weight, poured into the molds and left to cure in an oven (Heratherm OGH60, Thermo Fisher, USA) at 70 °C for 2 hours. Once cured, the PDMS was removed from the mold.

Force-extension curves were measured with an extension-controlled universal tester (Tinius Olsen 5ST, UK) equipped with a 250 N load cell. For the PDMS samples, the extension speeds were 10 mm min^{-1} in tension and 5 mm min^{-1} for the smaller compression samples. For Flexible Resin, the extension speeds were 20 mm min^{-1} in

tension and 3 mm min^{-1} in compression. For Durable Resin, the extension speeds were 20 mm min^{-1} in tension and 3 mm min^{-1} in compression. These rates, lower than suggested by testing standards [7,8], were chosen to be more representative of the strain rate applied on the sensors described in this paper. Eccentric roller grips and 5 cm diameter compression plates were used to fix samples.

Non-linear least-squares fitting was then carried out in COMSOL's Optimisation module and Microsoft Excel. A cost function, evaluating the difference between measured and fitted curves, was minimised to identify optimal parameters for the Neo-Hookean, Mooney-Rivlin, Ogden and Yeoh hyperelastic models [9].

Finite Element Modelling of PDMS-Based Sensors for Optimisation of Sensor Design

To increase the range of forces that the sensors can measure, a variety of modifications were made to the design of the sensor, including the reservoir width and height, the channel height, the number of columns and the PDMS curing ratio. These were compared with experimental calibration data.

Finite Element Modelling (FEM) was conducted using COMSOL Multiphysics 5.4 (COMSOL Inc., USA), a Finite Element Analysis (FEA) software, to optimise the sensor design before manufacture, to improve both the device sensitivity and increase the range of forces to achieve the 450 N target. The sensor was not modelled as a single model, as this would require analysis of fluid dynamics and electrostatics in response to mechanical deformation, which is both complex to model and computationally demanding.

The main manuscript Fig. 2 shows a simulation of the trial insert geometry. Two additional models were produced to simulate the response of an individual sensor to an applied load. The *electrode model* simulates the response of the electrodes (including capacitance values) when several parameters are varied, including the length of the liquid covering the electrodes, the shape of the electrodes and the type of liquid. The length of fluid displaced along the channel is converted into a capacitance value. The *reservoir deformation model* simulates the deformation of the reservoir as a force is applied. We model the effects of different reservoir geometries, varying the width, height, number and shape of columns, reservoir material, and PDMS curing ratio. The applied force is converted into a change in internal volume of the reservoir, which in turn is equivalent to the volume of fluid displaced along the channel. To simulate the deformation of PDMS, the Mooney-Rivlin 5-parameter hyperelastic model was considered most suitable for the range of strains obtained in the model [10] (see Figs. S5 and S6 for the fitting of hyperelastic deformation models to the microfluidic chip materials). Modelling the sensor response in planar geometries was covered in the group's previous work [11] – in this study, the sensor modelling is conducted using the curved implant geometry.

Reservoir deformation model (Fig. S1a): To model the deformation of the reservoir as a force is applied, in particular calculating the change in volume of the reservoir (and therefore, of the fluid). The effects of different reservoir geometries were calculated, including varying the width, height, number and shape of columns, and reservoir material

(including PDMS curing ratio). The effect of curvature was also considered, resembling the insertion of the sensor in the implant geometry. Simulations were performed using COMSOL's Structural Mechanics module. For this model, the volume was calculated by integrating the internal surfaces of the reservoir. The boundary conditions were a compressive force on the top surface and a fixed bottom surface, although the sides were also fixed in one simulation to determine the effect of enclosing the sensors in the grooves. The PDMS itself was modelled as a hyperelastic material, using the Mooney-Rivlin 5 parameter model, with the parameter obtained from mechanical testing (see Table S1). A free tetrahedral mesh was applied - the element sizes were generally around 0.25 mm, but the reservoir boundary concentrated more stress and so was meshed more finely at 0.09 mm.

Electrode model (Fig. S1b): The reservoir model outputs a change in volume of the reservoir under applied stress, which is equivalent to a volume of displaced dielectric liquid. The electrode model then determines the change in capacitance when this volume of fluid covers the interdigitated electrodes, resulting in a relationship between the applied force and the capacitance of the sensor. This was conducted using COMSOL's Electrostatics module. In this case, the boundary conditions were grounding one of the electrodes while raising the other to a potential of 1 V, and grounding the surrounding environment. The free tetrahedral mesh had a small element size of 0.0075 mm for the electrodes. The effect of curving the electrodes to the radius of the acetabular cup was determined.

PDMS-Based Sensor Fabrication

The PDMS-based sensors were manufactured in a different way to those made from Flexible Resin, in that the microfluidic chip was made by pouring PDMS into a 3D-printed mould.

PDMS microfluidic chip fabrication: a mold was printed using an SLA 3D printer (Form 3 Formlabs, USA) using Formlabs' proprietary Grey resin. The CAD file for the molds was custom-designed using Creo Parametric (PTC, USA), and the smallest layer thickness of 25 µm was chosen. After printing, the mold was washed in isopropanol in a sonicating bath for 15 minutes to remove excess resin. The mold was then cured in an oven (FormCure, Formlabs, USA) at 60 °C for one hour. PDMS (Sylgard 184, Dow, USA) was mixed with curing agent in a 10:1 ratio by weight, poured into the mold and left to cure in an oven (Heratherm OGH60, Thermo Fisher, USA) at 70 °C for 2 hours. Once cured, the PDMS was removed from the mold and cut to the appropriate size.

Bonding PDMS to Kapton [11]: a thin layer of primer (DOWSIL PR-1200 RTV Prime Coat, Dow, USA) was first applied on the surface of the Kapton film and left for 1 hour until fully dried. A thin layer of silicone sealant (DOWSIL 3140, Dow, USA) was applied on top of the primer, taking care not to cover the electrodes, and then attached to the PDMS microfluidic chip. The alignment between the PDMS and Kapton was then checked under an optical microscope. In order to minimise air bubbles between the PDMS and Kapton layers, a weight was put on top of the PDMS layer to press the two layers as the glue cured. The glue was then left to cure for a few hours.

Fluid injection: Once the glue has cured, a hole was made in the PDMS layer using a syringe. The hole is located adjacent to the reservoir but at the opposite end to the channel. The fluid, a 2:1 by volume glycerol-water mixture, was injected until it just filled the reservoir. The ratio was chosen in order to obtain a balance between a low volatility and high dielectric constant. The hole was then resealed with the silicone sealant.

The fabrication of the electrode layer is unchanged from the Flexible Resin sensors, and thus its fabrication details are given in the main manuscript.

Experimental Characterisation and Optimisation of PDMS-Based Sensor Design

Calibration and Fatigue Properties: Capacitance-force calibration was conducted using a linear motor (LinMot, Switzerland), the setup of which can be seen in Fig. S2. The pressing arm was made from a flat-head screw with a nitrile rubber sheet wrapped around it. The sensor was then attached between the pressing arm and the load cell. To apply load to the sensor, the linear motor was programmed to advance the pressing arm in intervals of 100 µm. To calibrate the sensor, forces read from the load cell were recorded while the impedance of the electrodes was monitored by an impedance analyser. The load cell was rated to read forces up to 20 N, although it was found in practice that this could go up to 40 N if a sufficient cooling system was put in place to stop it from overheating.

In order to determine the optimal design for the microfluidic chip, a variety of chip parameters were varied, including: channel dimensions; reservoir dimensions and shape; the presence, size and cross-sectional shape of supporting columns; and PDMS curing ratio. Each of the sensors with a different design was calibrated using the linear motor up to 20 N.

In addition, the fatigue properties of a typical sensor were investigated. An oscillating force between 0 - 11.67 N was applied to a PDMS-based sensor using the linear motor, with the pressing arm speed set at 0.584 mm s^{-1}, with the aim to reach 100 loading cycles before significant change in device performance.

Results

Experimental Mechanical Characterisation of Sensor and Insert Materials

PDMS: The effect of varying the PDMS curing ratio is given in Fig. S3. A lower curing ratio of PDMS led to slightly decreased sensitivity, both in simulations and experiments. Surprisingly, the mechanical properties of 5:1 and 10:1 PDMS were similar in compression, leading to similar responses of sensors made from 5:1 and 10:1 ratio PDMS.

Flexible Resin: Fig. S5 shows fitting of Mooney-Rivlin hyperelastic models to experimental stress-extension ratio data. The calculated hyperelastic parameters from optimisation are given in Table S2.

Durable Resin: Using the linear region of the stress-strain curve in Fig. S6, the Young's modulus of Durable Resin is approximately 162 MPa, although other sources indicate a much higher modulus of 1.0 GPa [1].

Finite Element Modelling of PDMS-Based Sensors for Optimisation of Sensor Design

Figs. S7-S10 show the effect of varying the sensor design. They indicate that the cross-sectional shape of the supporting columns has very little effect on the sensitivity. The most important feature is the volume of liquid in the reservoir that can be displaced into the channel, which depends on properties such as the number of columns and reservoir width and height.

The effect of changing the shape of the supporting columns, or removing the columns entirely, is shown in Fig. S9. PDMS with a 10:1 curing ratio was assigned as the microfluidic chip material. The reservoir had a square cross-section (w_{res} = 2 mm) and the supporting columns had either square or circular cross sections, or were absent entirely. Removing the columns decreases the complexity of fabrication, as it is easier to fill the channel with fluid by avoiding air bubbles, and is less computationally complex to simulate. The disadvantage to removing the columns for PDMS-based devices is the mechanical stability – the columns prevented the reservoir from collapsing in on itself when high forces were applied. Due to the increased stiffness, Flexible Resin-based devices did not have this issue and therefore the columns were not used.

In addition, 15 mm curvature was introduced to both the reservoir and electrode models to determine the effect of curvature on sensor response. In the electrode model, the sensitivity increased by less than 0.5%, from 9.43 to 9.46 pF μL^{-1} (negligible compared to other factors e.g. choice of mesh size).

Fig. S11 shows the effect of applying a lateral constraint to the deforming reservoir, to simulate the sensor being 'constrained' in the cup grooves.

Fig. S12 is a simple comparison of PDMS to common polymers that could be used to replace it as the microfluidic chip material.

PDMS-Based Sensor Fabrication

Optimisation of printing method: The group's previous work into fabricating the PDMS part of the device consisted of an AJP-based method, whereby NaCl salt was printed to form a sacrificial mold, PDMS was poured on top and cured, the resulting PDMS chip peeled off and the NaCl dissolved away [11]. This method reliably reproduced the square reservoir design, but the NaCl was difficult to dissolve as a PDMS-NaCl foam was deposited at the surface of the mold, often blocking the reservoir and making it difficult to fill with liquid. The foam can be removed, but this issue limits scalability and device reliability. In this paper, we present a new method. Molds were printed using the Formlabs Form 3 SLA printer and used to produce the devices as detailed in the Methods section. Although the SLA printer has a lower resolution (25 μm) compared to the AJP (10 ± 1 μm), and the SLA molds took longer to produce (18 hours for a single mold for SLA, vs 3 hours for six molds for AJP), the SLA molds could be reused, which significantly decreased sensor production time overall. One disadvantage is that a new mold must be produced for each modification to the design. However, perhaps the greatest advantage of SLA for this application is that the microfluidic chip can be printed directly, using Flexible Resin for example, without the need of a mold.

Experimental Characterisation and Optimisation of PDMS-Based Sensor Design

Sensor Calibration and Design Optimisation

Experimental calibration of PDMS-based sensors with different microfluidic chip designs are shown in Fig. S13.

Channel dimensions: Increased channel width or height leads to reduced sensitivity, as the larger cross sectional area of the channel would mean that the length of electrodes covered by liquid would be smaller for a certain applied force. Simulations were conducted with the same length of liquid covering the electrodes, but different channel width and height - as predicted, the capacitance values were near-identical (within 2%) for all channel widths above 0.5 mm (the electrode separation) and channel heights above 0.3 mm. Experimental results may also indicate this, as shown in Fig. S13. When comparing 0.25 mm- and 0.5 mm-wide channels, the former has a plateau of low sensitivity followed by the fluid reaching the end of the channel. Therefore, the channels could be made wider to incorporate a larger volume of liquid and go to higher forces, at the cost of sensitivity.

Reservoir dimensions: Increasing the width and height of the reservoir leads to greater sensitivity, as more fluid is expelled at a certain force. However, taller reservoirs had a smaller rate of fluid expelled per unit force, meaning that the corresponding sensors can withstand comparatively higher forces before the reservoir empties of fluid. This relationship did not hold for wider reservoirs, as can be seen from a plateau in sensitivity at low forces. Increasing the reservoir width increases the difficulty in filling the reservoir

completely – often the fluid enters the channel before filling the reservoir, leading to air bubbles.

Reservoir shape: In the group's previous work [11], a square reservoir was used. In this paper, it has been judged that circular cross-section reservoirs have the advantage of being easier to fill with fluid (preventing air bubbles) with the change in reservoir shape also having a insignificant effect on the sensitivity.

Presence of Columns: In the group's previous work [11], columns were used to provide mechanical stability and prevent collapse of the channel. For Flexible Resin-based devices the columns are no longer needed, perhaps in part due to the stress shielding provided by the implant geometry, and due to the increased stiffness of Flexible Resin. Furthermore, when fabricating the PDMS-based sensors it was difficult to fill the reservoir without producing air bubbles in part due to the presence of the columns obstructing fluid flow down the sides of the reservoir. This issue causes inconsistent readings and lack of sensor consistency of measurements.

Square vs Round columns: This was investigated during modelling, but has not been verified experimentally yet. Modelling results are as follows: the increase in volume of the reservoir (i.e. the rounded columns are smaller than the square ones because their diameter = side of square) has more of an effect than the reservoir shape. Peak stress concentrations near reservoir columns reduced from 1.64 MPa to 981 kPa under 6 N of force.

The optimal design changes to make based on these results are to increase the channel and reservoir height. Increasing the length is also an option, but to achieve a large spatial resolution the sensor must be as small as possible. Options include creating a serpentine channel and electrodes.

Fatigue Properties

The fatigue experiment results can be seen in Fig. S14 - the sensor lasted up to at least 100 cycles without significant change in device performance. Previously, it has been shown that these sensors are durable over at least 2000 cycles [11].

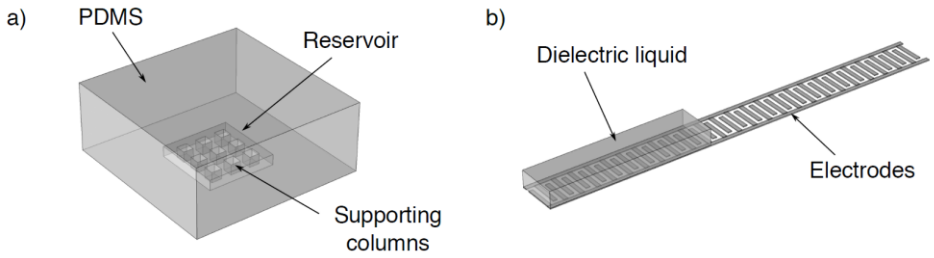

Fig. S1.
Visualisation of studied FEM geometries. (A) The reservoir model, which consists of a fluid reservoir (Length x Width x Height: 2 mm x 2 mm x 0.3 mm) embedded in a soft elastomer such as PDMS (5 mm x 5 mm exposed area). **(B)** The electrode model (20 mm electrode length, 0.1 mm electrode width and separation, 0.5 mm x 0.2 mm channel cross-section).

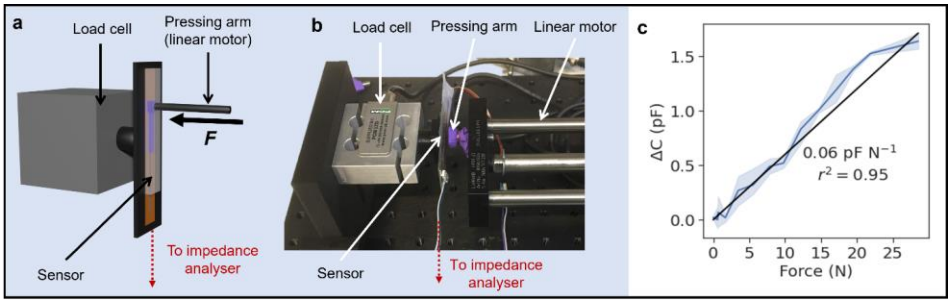

Fig. S2.
Calibration of sensors using a linear motor. (A) Schematic diagram of linear motor operation – a pressing arm exerts a force on the sensor, which is adhered to a load cell to measure the applied force. The sensor impedance is measured with an impedance analyser. **(B)** Photograph showing one sensor in the linear motor setup. **(C)** Typical calibration of a Flexible Resin-based sensor using the linear motor.

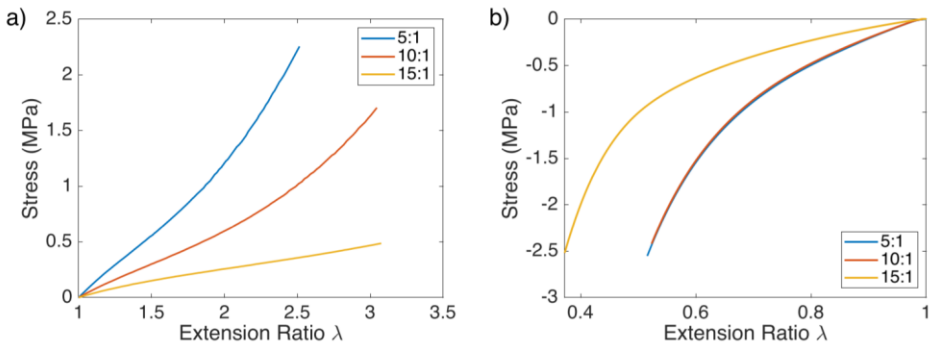

Fig. S3.
Experimentally measured mechanical properties of PDMS at different curing ratios. **(A)** Uniaxial tension, carried out to failure. **(B)** Compression, terminated near the limit of the load cell range at 200 N.

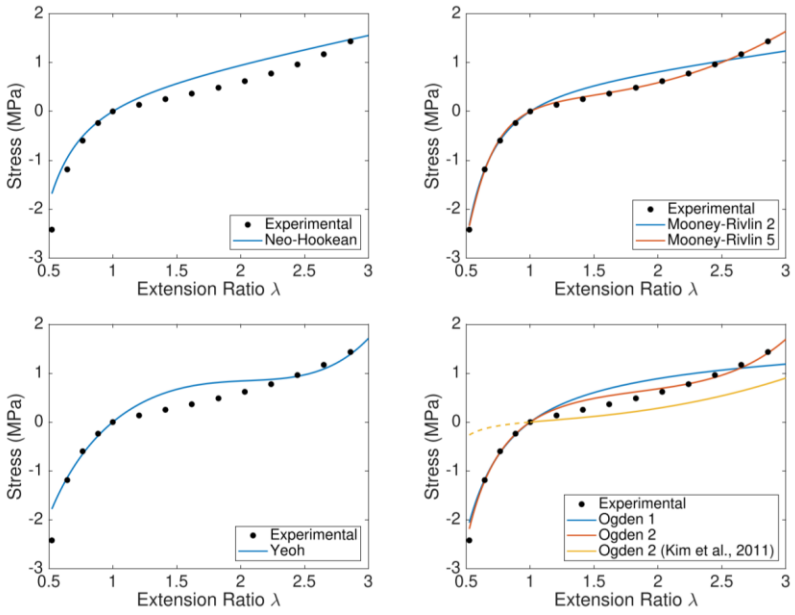

Fig. S4.
Hyperelastic models fitted to the experimental stress-extension ratio curve for 10:1 PDMS. For comparison, the best-fit numerical curve from Kim *et al.* (2011) [12], Ogden 2nd order, is included and extrapolated in compression.

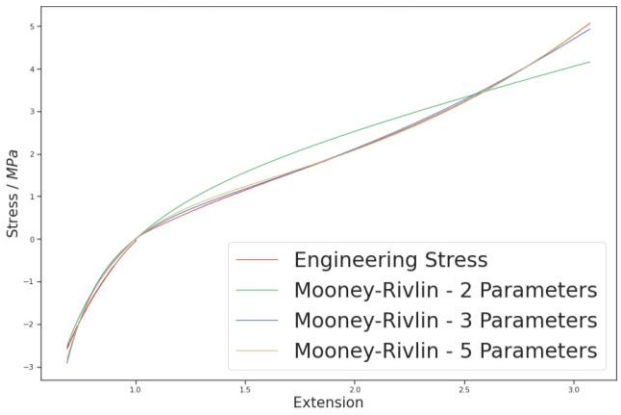

Fig. S5.
Mooney-Rivlin hyperelastic models fitted to the experimental stress-extension ratio curve for Flexible Resin.

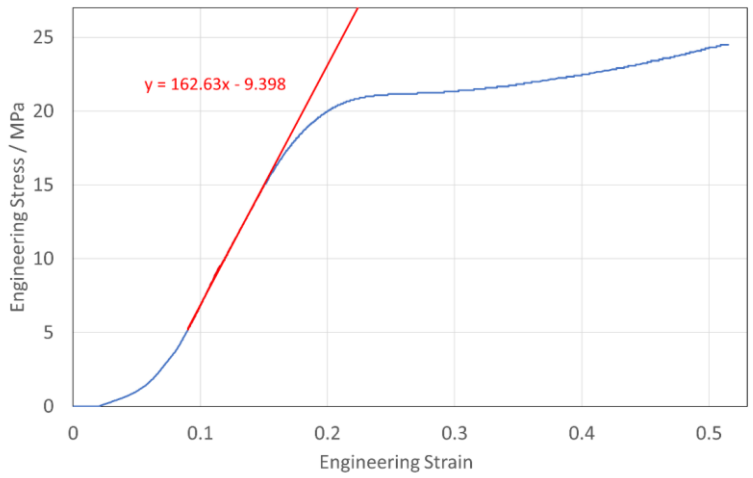

Fig. S6.
Engineering stress-strain curve for Durable Resin. The behaviour is non-linear at very low and high strains, with an approximately linear region in-between.

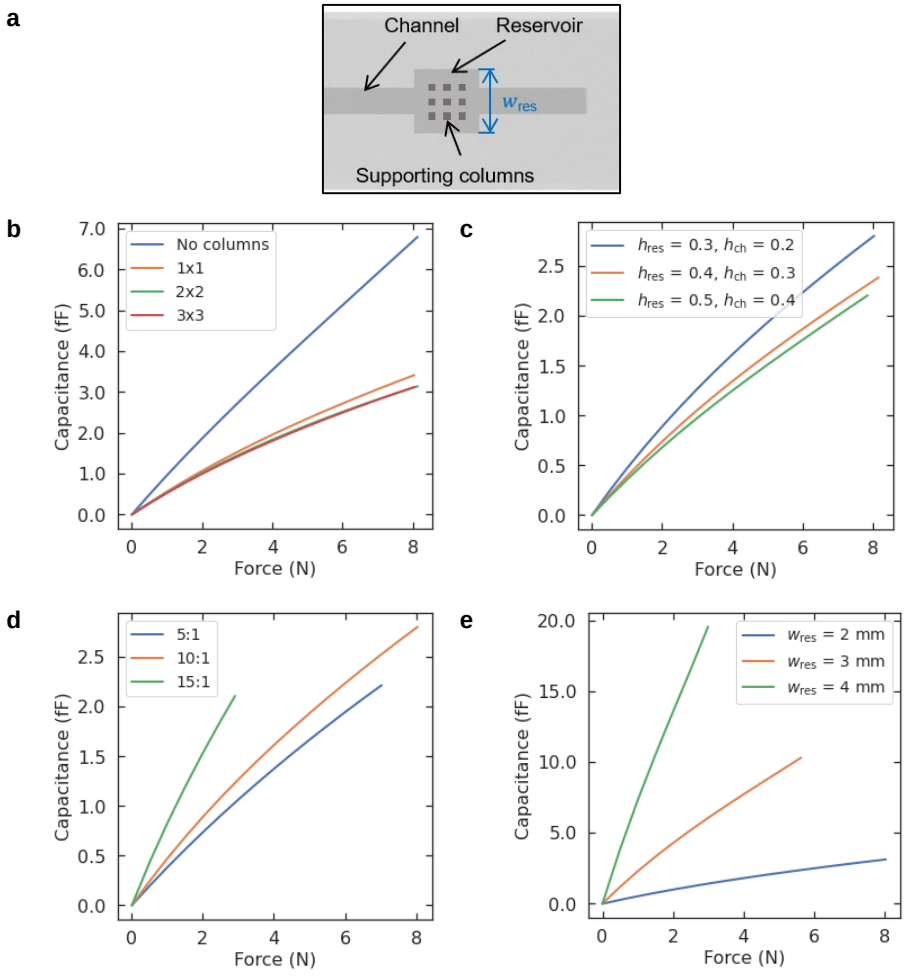

Fig. S7.
Effect of changing reservoir design on sensor sensitivity, for a reservoir supported by square cross-section columns. For most simulations, the model could not converge past 8 N. For other simulations, convergence failed at lower forces. **(A)** Schematic of the reservoir, showing the supporting columns. **(B)** Effect of varying the number of columns. **(C)** Effect of varying the reservoir height h_{res} and channel height h_{ch}. **(D)** Effect of varying the ratio of PDMS base to curing agent (by mass). **(E)** Effect of varying the width of the square reservoir, w_{res}.

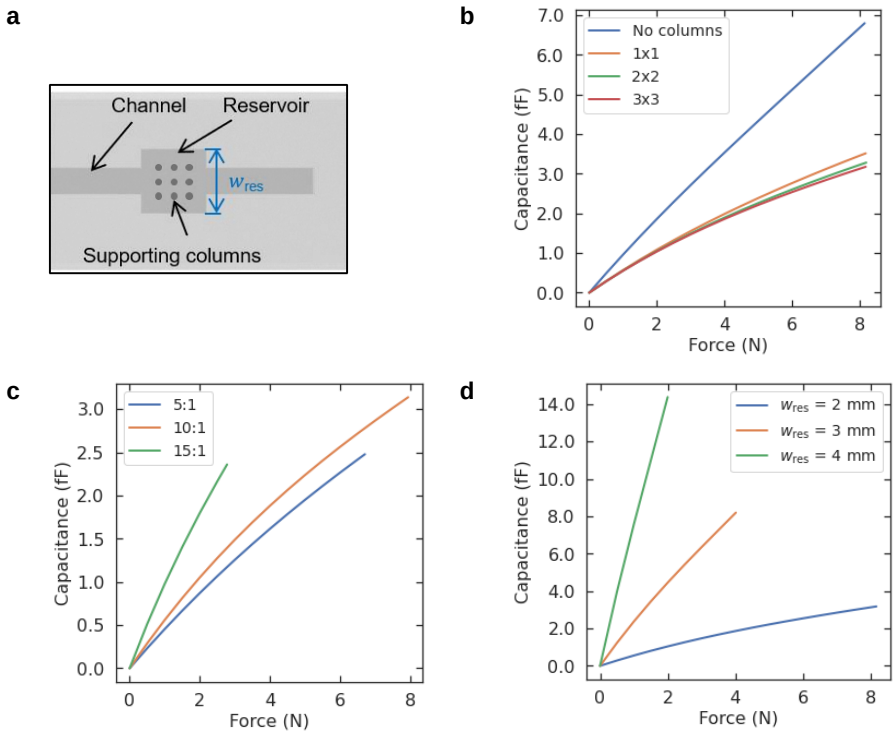

Fig. S8.
Effect of changing reservoir design on sensor sensitivity, for a reservoir supported by circular cross-section columns. For most simulations, the model could not converge past 8 N. For other simulations, convergence failed at lower forces. **(A)** Schematic of the reservoir, showing the supporting columns. **(B)** Effect of varying the number of columns. **(C)** Effect of varying the PDMS curing ratio. **(D)** Effect of varying the width of the square reservoir, w_{res}.

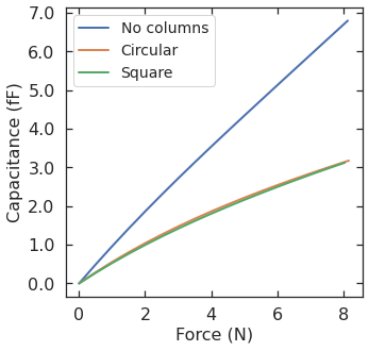

Fig. S9.
The effect of changing the cross-sectional shape of the supporting columns, showing the effect of having square columns, circular columns, or no columns at all. Note that as per Figures S6 and S7, the column cross-sectional shape has little effect.

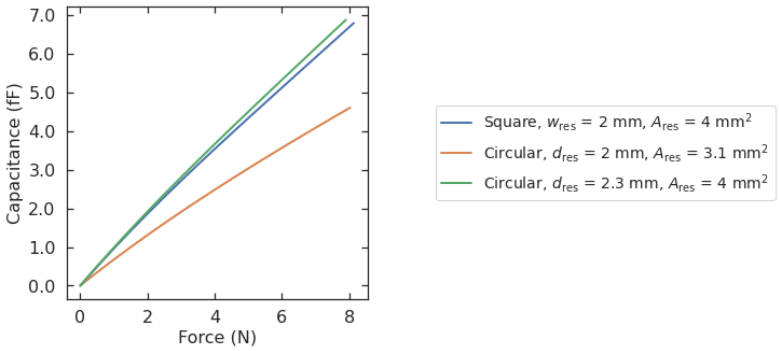

Fig. S10.
Showing the effect of changing the reservoir shape on the sensitivity. This figure compares the effect of a square cross-section with width w_{res} = 2 mm (blue), a circular cross-section with a diameter d_{res} = 2 mm (orange), and a circular cross section with the same cross-sectional area A_{res} as the square reservoir (green). The two simulations with the same reservoir cross-sectional area have similar responses. The reservoirs in this simulation have no supporting columns.

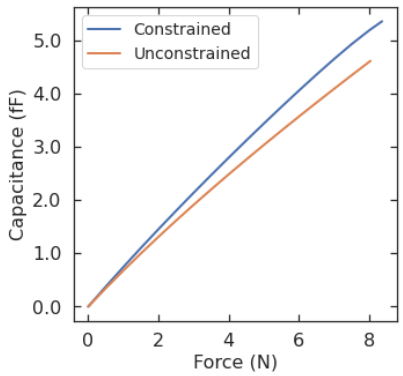

Fig. S11.
Applying a lateral constraint to the deforming reservoir, to simulate the sensor being 'constrained' in the cup grooves.

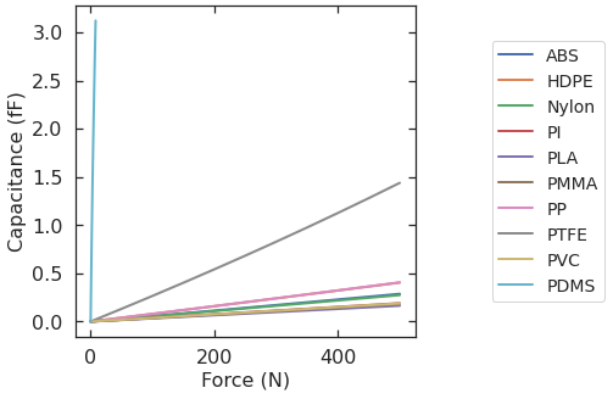

Fig. S12.
Brief comparison of PDMS to other common polymers. PDMS is simulated as a hyperelastic material, the others are treated as linear elastic. Due to its relatively low stiffness, a PDMS sensor would exhibit a greater fluid displacement per unit force, leading to a larger capacitance change for low forces.

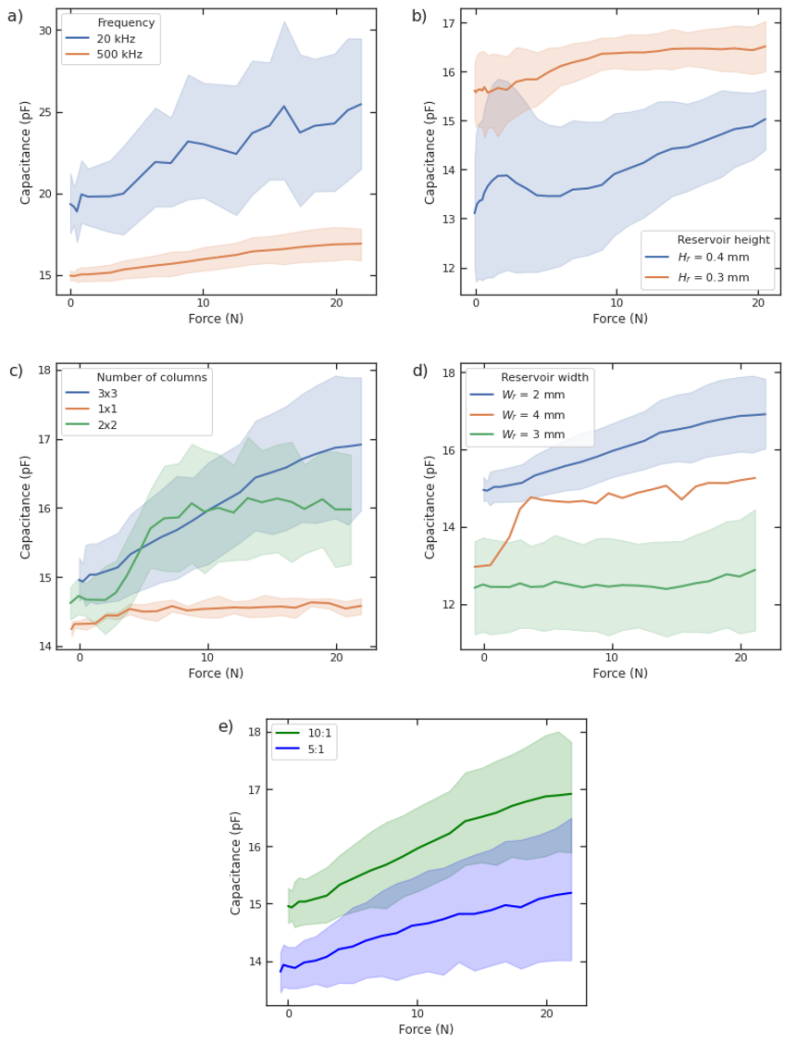

Fig. S13.
Experimental calibration of PDMS-based sensors up to 20 N, varying different sensor parameters. The shaded areas represent the 95% confidence interval from repeat experiments (repeat data was not available for some samples). **(A)** Frequency: A smaller measurement frequency results in a greater sensitivity but smaller signal to noise ratio. **(B)** Reservoir and channel height: a larger reservoir increases the sensitivity. **(C)** Number of columns: increasing the number of columns increases the sensitivity. **(D)** Reservoir width: increasing the reservoir width has little effect on the sensitivity. **(E)** Curing ratio: 10:1 and 5:1 curing ratios have similar sensitivities.

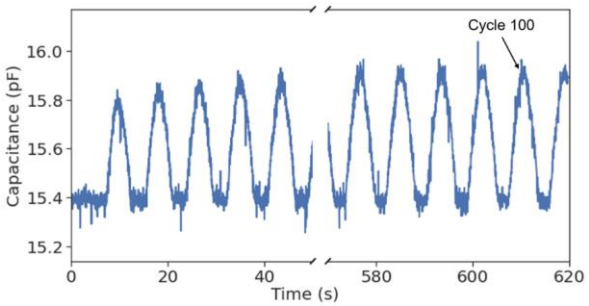

Fig. S14.
Effect of repeated loading on sensor performance. The sensor exhibited a consistent capacitance response beyond 100 cycles.

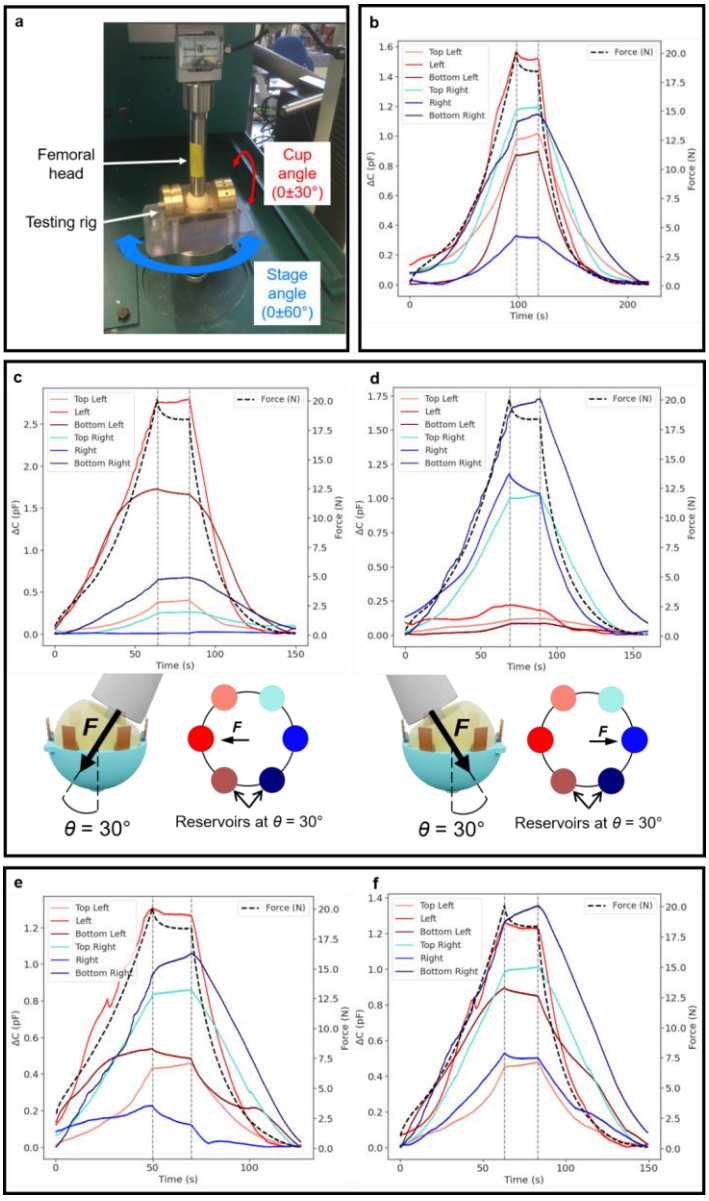

Fig. S15. Effect of varying cup and stage angles. (A) Experimental testing of the rig setup. The cup angle is the angle between the applied force and the normal to the plane of the cup. The stage angle is the lateral rotation of the rig. **(B)** Capacitance change with

applied force (up to 20 N) over time for six sensors in the testing rig, with the cup and stage angles at 0°. The sensors are labelled based on their relative position in the cup. **(C),(D)** Rotating the cup angle θ to ±30°. **(E),(F)** Rotating the stage angle to ±60°.

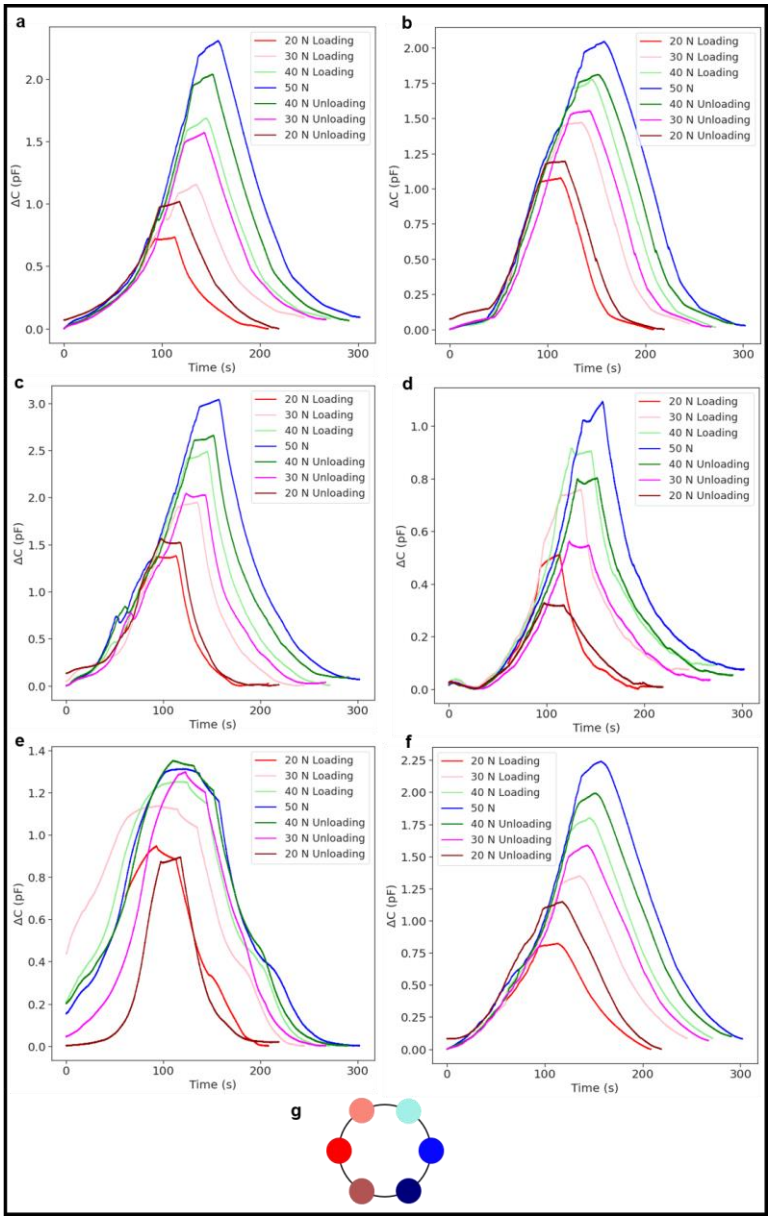

Fig. S16.
Repeated loading of six sensors, in the **(A)** top left, **(B)** top right, **(C)** left, **(D)** right, **(E)** bottom left and **(F)** bottom right positions in the cup. The maximum force reached in a

loading cycle was increased from 20 N to 50 N in steps of 10 N, then decreased to 20 N. **(G)** The sensors (represented by coloured dots) were located 60° apart from each other.

Reduced chi-squared, χ_R^2	PDMS Curing Ratio		
	5:1	**10:1**	**15:1**
Neo-Hookean	22.73	7.24	480.0
Mooney-Rivlin, 2 parameters	23.61	2.83	30.75
Mooney-Rivlin, 5 parameters	3.20	0.96	47.67
Yeoh	12.33	8.59	546.7
Ogden, 1st order	17.96	5.24	136.0
Ogden, 2nd order	5.67	2.67	96.40

Table S2.
Reduced chi-squared values for different hyperelastic models fitted to measured stress-extension ratio curves. Values significantly greater than 1 indicate poor fit whereas values smaller than 1 show overfitting with respect to experimental error.

	Mooney-Rivlin 2-Parameter	Mooney-Rivlin 3-Parameter	Mooney-Rivlin 5-Parameter
Parameter	Value / MPa	Value / MPa	Value / MPa
C_{10}	0.62691	0.10901	0.19850
C_{01}	0.36902	0.58551	0.58126
C_{11}	N/A	0.09690	0.00001
C_{20}	N/A	N/A	0.03392
C_{02}	N/A	N/A	0.00000

Table S3.
Calculated Mooney-Rivlin parameters that provide the best fit for the stress-extension data for Flexible Resin.

[1] Materials Data Sheet Photopolymer Resin for Form 1+ and Form 2, 2018.
[2] I.D. Johnston et al., Mechanical characterization of bulk Sylgard 184 for microfluidics and microengineering, OPEN ACCESS Journal of Micromechanics and Microengineering J. Micromech. Microeng. 24 (2014) 1–7. https://doi.org/10.1088/0960-1317/24/3/035017.
[3] J.W. Swanson et al., The effect of implantation on the physical properties of silicone rubber, Journal of Biomedical Materials Research. 8 (1974) 357–367. https://doi.org/10.1002/jbm.820080603.
[4] G.C. Randall et al., Permeation-Driven Flow in Poly(Dimethylsiloxane) Microfluidic Devices, Source. 102 (2005) 10813–10818. https://doi.org/10.1073/pnas.0503287102.
[5] M.W. Toepke et al., PDMS absorption of small molecules and consequences in microfluidic applications, Lab on a Chip. 6 (2006) 1484–1486. https://doi.org/10.1039/b612140c.
[6] O. Müller et al., Three-dimensional measurements of the pressure distribution in artificial joints with a capacitive sensor array, Journal of Biomechanics. 37 (2004) 1623–1625. https://doi.org/10.1016/j.jbiomech.2004.01.024.
[7] ASTM D575 - 91(2018) Standard Test Methods for Rubber Properties in Compression, (n.d.). https://www.astm.org/Standards/D575.htm (accessed April 12, 2021).
[8] ASTM D412 - 16e1 Standard Test Methods for Vulcanized Rubber and Thermoplastic Elastomers—Tension, (n.d.). https://www.astm.org/SUBSCRIPTION/filtrexx40.cgi?+REDLINE_PAGES/D412.htm (accessed April 12, 2021).
[9] A.H. Muhr, Modeling the stress-strain behavior of rubber, Rubber Chemistry and Technology. 78 (2005) 391–425. https://doi.org/10.5254/1.3547890.
[10] M. Shahzad et al., Mechanical Characterization and FE Modelling of a Hyperelastic Material, 18 (2015) 918–924.
[11] Q. Jing et al., Aerosol-jet-printed, conformable microfluidic force sensors, Cell Reports Physical Science. 2 (2021) 100386. https://doi.org/10.1016/j.xcrp.2021.100386.
[12] T.K. Kim et al., Measurement of nonlinear mechanical properties of PDMS elastomer, in: Microelectronic Engineering, Elsevier, 2011: pp. 1982–1985. https://doi.org/10.1016/j.mee.2010.12.108.